Molecular Lifetime Changes Induced by Nanometer Scale Optical Fields

Christian Girard

Laboratoire de Physique Moléculaire UA CNRS 772, Université de Franche Comté, 25030 Besançon, France

Olivier J. F. Martin

Swiss Federal Institute of Technology, ETH-Zentrum, 8092 Zurich, Switzerland

Alain Dereux

Institute for Studies in Interface Sciences, Facultés Universitaires, N.-D. de la Paix, 5000 Namur, Belgium
(Received 4 May 1995)

We present a new practical scheme to study the spectroscopic properties of molecules embedded in optically complex surroundings. The response function accounting for the modification of the spectroscopic behavior of the molecules is derived self-consistently in direct space through the numerical solution of Dyson's equation. We apply this scheme to investigate near-field optical effects due to fluorescence phenomena. Experimentally relevant examples show that the dramatic decay of the molecular lifetime upon approaching a surface defect could achieve well-resolved imaging of subwavelength structures.

PACS numbers: 33.80.–b, 42.30.Yc, 78.66.–w, 85.42.+m

The decay of the fluorescence lifetime of an excited molecule in interaction with a solid surface has been extensively studied over the last twenty years [1–4]. In the past few years, the interest for this proximity effect has been revived by the emergence of new optical characterization methods able to analyze spectroscopic events associated with individual molecules [5–11]. More recently, scanning near-field optical microscopy (SNOM) performed with a subwavelength aperture has been successfully used to image the fluorescence near-field signal emitted by a single molecule [7–9]. These contributions raised several important questions concerning the mechanisms underlying such experiments: How does the macroscopic surrounding formed by the tip-sample junction modify the behavior of the embedded quantum system? In particular, what kind of relation between image and object may be expected by measuring the lifetime changes of a molecule attached to the probing tip?

From a theoretical point of view, this new experimental methodology is challenging because of the limited number of predictive models able to describe the modification of the intrinsic spectroscopic properties of molecules in the presence of mesoscopic structures dressed with complex optical surroundings [11]. In fact, the presence of any microscopic system (here the molecules) placed in interaction with a mesoscopic environment breaks down the symmetry. This makes the application of a standard boundary conditions based method extremely difficult. This difficulty can be overcome by a combination of microscopic and macroscopic descriptions, where the response function of the dielectric surrounding is derived from an appropriate iterative numerical algorithm [12].

The aim of this Letter is twofold. First, we will adapt the well-established electromagnetic field propagator method to some experimentally relevant configu-rations (SNOM junctions or nanocavity with interacting molecules). In our scheme, we will neglect any effect originating from the specific chemical interactions between the molecule and its surrounding. In a second stage we will extract the effective polarizability of the molecule dressed by the local electromagnetic field [13].

Let us consider a junction formed by the tetrahedral tip of a SNOM device facing a bare dielectric surface. When such a low symmetry system is excited by an external optical field, a highly confined field appears at the vicinity of the tip. Figure 1 illustrates such a nanometer-size optical field produced in the gap region of a SNOM junction. This computer simulation was performed with the numerical scheme described in [14]. Such subwave-
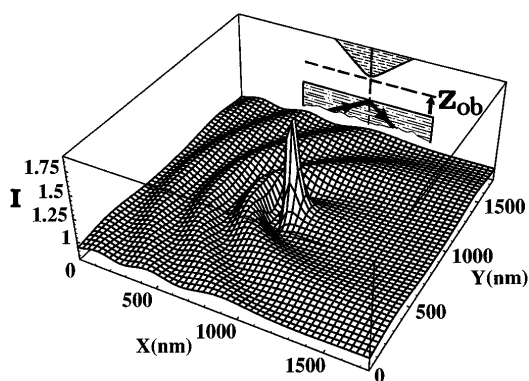

FIG. 1. Illustration of scattering and light confinement in the vicinity of a SNOM junction [14]. The three-dimensional map represents the normalized field intensity $I = |E|^2/|E_0|^2$, calculated in the observation plane $Z_{obs} = 20$ nm. The tip-sample distance is 30 nm and the system is illuminated in internal reflection in the p-polarized mode. The optical indexes of tip and sample are identical ($n = 1.5$) and the incident wavelength $\lambda = 600$ nm. In the present configuration, the FWHM of the peak reaches about 75 nm.

length confinement effect is typical of SNOM devices and cannot be achieved with usual optical focusing. Because of this strong confined field, nanometric spatial variations of the dielectric surrounding will also modify the intrinsic polarizability of a molecule placed in its proximity. This introduced then a significant modification of the lifetime of the excited molecular level, always accompanied with a small shift of the corresponding occupied level [13]. These spectroscopic changes can be qualitatively understood by saying that the molecule is "dressed" by the surrounding, or, in other words, that the molecule responds with an *effective polarizability* $\alpha^{\text{eff}}(\omega)$. In the case of a planar surface, the lifetime variation of the excited state depends on the distance between the molecule and the surface in a rather complex manner. At very large distances, this variation displays an oscillatory regime due to interference phenomena; whereas in the near zone, the nonradiative energy transfer between the excited molecule and the surface produces a strong decrease of the lifetime [1]. There are actually some similarities between this phenomenon and the nonradiative optical energy transfer exploited in the optical tunneling effect [15]. Indeed, both of them are governed by evanescent optical fields.

Let us now analyze how the intrinsic response properties of the molecule are perturbated by a nanoscale dielectric environment. When the junction is excited with the optical field $\mathbf{E}_0(\mathbf{r}, t)$ of an external laser source, the local field $\mathbf{E}(\mathbf{r}, t)$ displayed in Fig. 1 is a physical observable, since it has already been averaged on the quantum states of the dielectric surrounding. This field can be computed from various direct space numerical schemes [14,16]. When a single molecule, labeled (**m**) and located at $\mathbf{r}_m$, is then introduced in the junction, the interaction Hamiltonian reads

$$H(t) = -[\mathbf{E}(\mathbf{r}_m, t) + \mathcal{E}(\mathbf{r}_m, t)] \cdot \mu(t), \quad (1)$$

where $\mu(t)$ and $\mathcal{E}(\mathbf{r}_m, t)$ are the polarization operator of the molecule and the electric field operator associated with the dielectric surrounding, respectively. These operators are written here in the interaction representation. At this stage, since we neglect any chemical interaction between the molecule and its support, we can assume that the short range interaction between the molecule and the dielectric surrounding does not cause any significant modification of the wave function $|\psi\rangle$ of the entire system. With this assumption it is legitimate to apply the time dependent Hartree approximation, where one assumes that each part of the system moves under the combined effect of the external force and the average displacement of the other parts [17]. One can then consider that $|\psi\rangle$ is a tensor product of the two wave functions $|\psi_{\text{mol}}\rangle$ and $|\psi_{\text{sur}}\rangle$ associated with the molecule and the surrounding, respectively. A straightforward application of the perturbation theory shows that the linear response of the two variables $\mu(t)$ and $\mathcal{E}(\mathbf{r}, t)$ is given by

$$\mathbf{E}_{\text{mol}}(\mathbf{r}_m, t) = \langle \mathbf{E}(\mathbf{r}_m, t) + \mathcal{E}(\mathbf{r}_m, t) \rangle$$
$$= \mathbf{E}(\mathbf{r}_m, t) + \int_{-\infty}^{t} \mathbf{S}(\mathbf{r}_m, \mathbf{r}_m, t - t') \cdot \langle \mu(t') \rangle \, dt' \quad (2)$$

and

$$\mu_{\text{mol}}(\mathbf{r}_m, t) = \langle \mu(t) \rangle$$
$$= \int_{-\infty}^{t} \alpha_0(t - t') \cdot \langle \mathbf{E}(\mathbf{r}_m, t') + \mathcal{E}(\mathbf{r}_m, t') \rangle \, dt', \quad (3)$$

where $\mathbf{E}_{\text{mol}}(\mathbf{r}_m, t)$ and $\mu_{\text{mol}}(\mathbf{r}_m, t)$ represent the temporal variation of the effective field and of the dipole moment at the position of the molecule, respectively. The dyadic tensor $\mathbf{S}(\mathbf{r}_m, \mathbf{r}_m, t - t')$ defines the temporal representation of the field susceptibility of the dielectric surrounding and $\alpha_0(t - t')$ the dynamical polarizability of the molecule. These quantities can be expressed in terms of the quantum average of the commutators of the operators $\mathcal{E}(\mathbf{r}, t)$ and $\mu(t)$ [18]:

$$\mathbf{S}(\mathbf{r}, \mathbf{r}', t - t') = (i/\hbar) \langle \psi | [\mathcal{E}(\mathbf{r}', t'), \mathcal{E}(\mathbf{r}, t)] | \psi \rangle \quad (4)$$

and

$$\alpha_0(t - t') = (i/\hbar) \langle \psi | [\mu(t'), \mu(t)] | \psi \rangle. \quad (5)$$

Finally, by replacing Eq. (3) in Eq. (2), one obtains the time dependent self-consistent equation for the molecular electric field:

$$\mathbf{E}_{\text{mol}}(\mathbf{r}_m, t) = \mathbf{E}(\mathbf{r}_m, t)$$
$$+ \int_{-\infty}^{t} dt' \int_{-\infty}^{t'} dt'' \mathbf{S}(\mathbf{r}_m, \mathbf{r}_m, t - t')$$
$$\times \alpha_0(t' - t'') \mathbf{E}_{\text{mol}}(\mathbf{r}_m, t''). \quad (6)$$

The solution of this implicit integral equation requires one to pass into ω space:

$$\mathbf{E}_{\text{mol}}(\mathbf{r}_m, \omega) = \mathbf{M}(\mathbf{r}_m, \omega) \cdot \mathbf{E}(\mathbf{r}_m, \omega), \quad (7)$$

where $\mathbf{M}(\mathbf{r}_m, \omega)$ is the (3×3) dynamical matrix defined by

$$\mathbf{M}(\mathbf{r}_m, \omega) = [\mathbf{I} - \mathbf{S}(\mathbf{r}_m, \mathbf{r}_m, \omega) \cdot \alpha_0(\omega)]^{-1}. \quad (8)$$

In a first stage, this equation gives the molecular effective field $\mathbf{E}_{\text{mol}}(\mathbf{r}_m, \omega)$. The field $\mathbf{E}_{\text{mol}}(\mathbf{r}_m, \omega)$ generated by the molecule far away from the molecule can be described by applying the matrix Lippmann-Schwinger equation associated with a single molecule [13,14]

$$\mathbf{E}_{\text{mol}}(\mathbf{r}, \omega) = \mathbf{E}(\mathbf{r}, \omega)$$
$$+ \mathbf{S}(\mathbf{r}, \mathbf{r}_m, \omega) \cdot \alpha^{\text{eff}}(\omega) \cdot \mathbf{E}_{\text{mol}}(\mathbf{r}_m, \omega), \quad (9)$$

with

$$\alpha^{\text{eff}}(\omega) = \alpha_0(\omega) \cdot \mathbf{M}(\mathbf{r}_m, \omega). \quad (10)$$

This renormalized response function describes how the molecule radiates optical energy when its polarizability is dressed by the surrounding junction. In our electrodynamical treatment, this proximity effect is completely

contained in the dyadic $\mathbf{S}(\mathbf{r}, \mathbf{r}', \omega)$ which is the key in-gredient of our problem [cf. Eqs. (8) and (10)]. In the past, various matching boundary conditions based meth-ods have been used for the calculation of $\mathbf{S}(\mathbf{r}, \mathbf{r}', \omega)$ near systems of simple symmetry (spheres, cylinders, planes, etc.) [13]. In the presence of highly complex optical sys-tems other strategies must be adopted. As discussed in [12,14], the recent developments of real space approaches for electromagnetic scattering and light confinement es-tablished a powerful tool for the calculation of the elec-tromagnetic response of arbitrary optical systems. In that scheme, the field-susceptibility tensor $\mathbf{S}$ required to obtain $\alpha^{\mathrm{eff}}(\omega)$ obeys the discretized Dyson's equation

$$\mathbf{S}(\mathbf{r}_i, \mathbf{r}_j, \omega) = \mathbf{S}_0(\mathbf{r}_i, \mathbf{r}_j, \omega)$$
$$+ \sum_{k=1}^{n} \chi_k(\mathbf{r}_k, \omega) \cdot \mathbf{S}_0(\mathbf{r}_i, \mathbf{r}_k, \omega) \cdot \mathbf{S}(\mathbf{r}_k, \mathbf{r}_j, \omega), \quad (11)$$

where the tip-sample system has been divided into n meshes of volume V_i centered at $\mathbf{r}_i, i = 1, \ldots, n$, and

$$\chi_i(\mathbf{r}_i, \omega) = [\epsilon(\mathbf{r}_i, \omega) - 1]V_i/4\pi \quad (12)$$

is related to the dielectric constant $\epsilon(\mathbf{r}_i, \omega)$. The dyadic $\mathbf{S}_0$ occurring in Eq. (11) defines the field susceptibility of a reference system (e.g., the surface of a dielectric [14]). Instead of solving Eq. (11) with a standard linear algebra procedure, we apply the original iterative procedure de-scribed in [12,16], which allows one to handle accurately very large discretized systems.

In the next stage, in order to avoid the huge computa-tional difficulties involved in an *ab initio* treatment of the dynamical properties of the molecule, we will restrict our discussion to a two-level molecular model [13]

$$\alpha_0(\omega) = \frac{1}{\hbar} \left\{ \frac{2\omega_0 \mu^{01}\mu^{01}}{\omega_0^2 - \omega^2 - i\omega\Gamma_0} \right\}, \quad (13)$$

where μ^{01} is the matrix element of the operator polar-ization between the two molecular levels. Using a simi-lar two-level representation for the effective polarizability and assuming that the dressed molecule belongs to the $C_{\infty v}$ molecular group, we can define two different effec-tive polarizabilities $\alpha_{\parallel}^{\mathrm{eff}}(\omega)$ and $\alpha_{\perp}^{\mathrm{eff}}(\omega)$. The symbol $\parallel$ refers to the emitting dipole direction parallel to the plane of the substrate, whereas $\perp$ refers to the emitting dipole direction orthogonal to that plane. The effective width associated with $\alpha_{\parallel/\perp}^{\mathrm{eff}}(\omega)$ can be obtained by introducing Eq. (13) in (10); this leads to

$$\Gamma_{\parallel/\perp}(\mathbf{r}_m) = \Gamma_0 \mathrm{Re} \left\{ \frac{\mathbf{M}_{xx/zz}(\mathbf{r}_m, 0)}{\mathbf{M}_{xx/zz}(\mathbf{r}_m, \omega_0)} \right\}. \quad (14)$$

Note that when the matrix $\mathbf{M}$ in Eq. (14) is expanded to the first Born approximation, one recovers a result previously discussed by Metiu [13].

In Fig. 2 we have used relation (14) to investigate the distance dependence of the normalized lifetime $\Gamma_0/\Gamma_{\parallel}$ for a fluorescing molecule located in the tip-sample junction. This quantity can be measured by generating a p-polarized surface wave with an electric field perpendicular to the
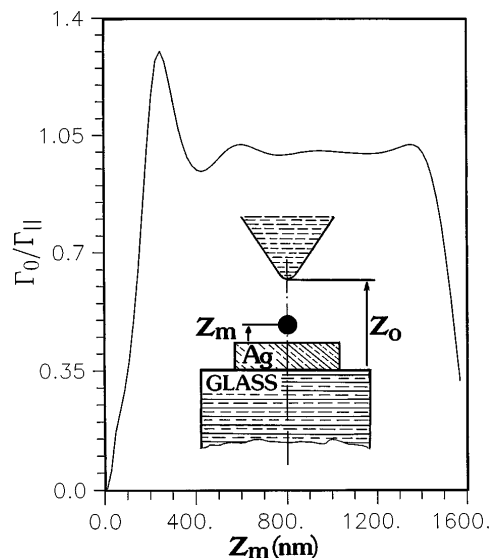

FIG. 2. Distance dependence of the normalized lifetime $\Gamma_0/\Gamma_{\parallel}$ inside the junction, as a function of the position of the molecule. The geometry used in the simulation is described in the inset and the tip-sample separation is maintained at $Z_0 = 1600$ nm. The glass sample is covered with a square shaped silver layer 300 nm long and 20 nm high.

surface of the sample [15]. The simulations presented in Figs. 2 and 3 are performed in this polarization mode. The molecular parameters used in this simulation are $\Gamma_0 = 2 \times 10^6 \ \mathrm{s}^{-1}$, $\alpha_0 = 10 \ \text{Å}^3$, and the fluorescing wavelength is $\lambda_0 = 612$ nm. The geometry of the junc-tion consists of a glass support with a thin square silver protrusion, facing a tetrahedral dielectric tip with sharp edges and a 10 nm ending curvature radius. When the molecule approaches the metal pad, one first observes the usual decay followed then by the fluorescence quenching. For intermediate distances, the lifetime variation in the gap region ($300 \leq Z_m \leq 1300$ nm) displays standard quasi-periodic oscillations with a period close to the half-fluorescing wavelength λ_0. It may be seen that towards the dielectric tip the decay is less abrupt, and a mag-nification of the evolution of the coefficient $\Gamma_0/\Gamma_{\parallel}$ as the molecule approaches the tip extremity indicates that the lifetime drops about 1 order of magnitude when the molecule becomes adsorbed on the tip surface. In this particular case where the material (here the glass sharp tip) does not display dissipative properties in the optical range, the decay originates from the specific form of the imaginary part associated with the spatial contribution of the tip propagator. In other words, this effect is related to the high model density existing in the near-field zone around such systems (cf. Fig. 1). Furthermore, when the tip is brought near the substrate the oscillations collapse. In such a situation, the molecular lifetime change, al-though sensitive to the combined action of the tip and of the sample, remains induced by the presence of the metal.

This first simulation clearly indicates that the fluoresc-ing molecule behaves as a highly sensitive nanoprobe to
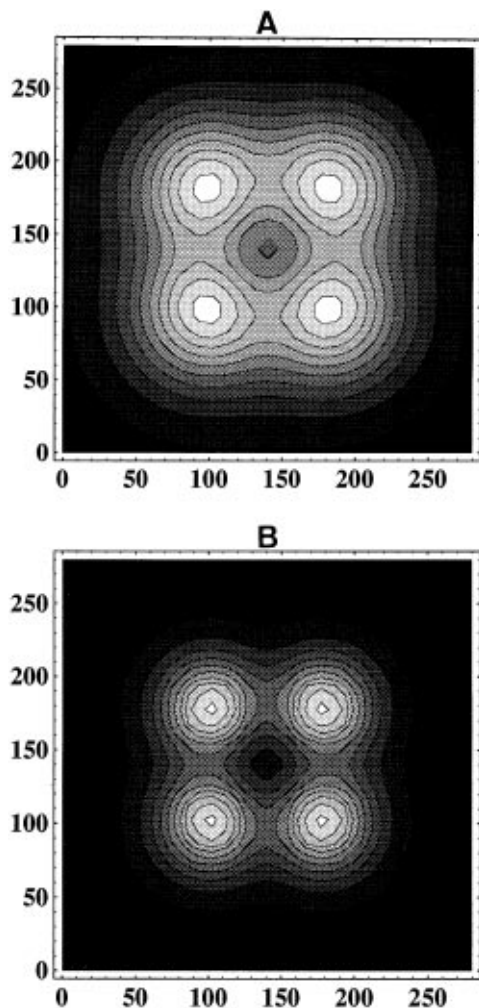
FIG. 3. Simulation of a sequence of two fluorescence NFI of a square shaped silver protrusion deposited on a glass substrate. The scan area is 280×280 nm^2 and two different approach distances are investigated: (A) $Z_0 = 80$ nm and η varies from 0.975 (black area) to 1.75 (white); (B) $Z_0 = 50$ nm and $0.984 \leq \eta \leq 5.3$.

the external environment. In particular, working in the near-field zone just before the quenching effect occurs, should make it possible to increase the lateral SNOM resolution [8]. We have further investigated this aspect and give in Fig. 3 a sequence of two fluorescence near-field images (NFI) of a square shape silver pad of section 90×90 nm^2 and 15 nm height. In this simulation, the molecule is attached to the extremity of the same tetrahedrally shaped probing tip with a 10 nm ending curvature radius. These images were obtained by calculating the normalized width $\eta = \Gamma_\parallel / \Gamma_0$ when the tip-molecule system is scanning above the sample. The evolution of the NFI against the tip-sample distance raises the following comments: First, one observes that the image remains symmetrical with respect to the object contour, whatever the tip-sample separation investigated. In fact, in the p-polarized illumination mode the symmetry of the NFI image is mainly governed by the decay of a moleclar dipole

perpendicular to the average plan of the sample. The main resulting effect is, as expected, a better image-object relation. This behavior differs from the usual SNOM configuration in which the near-field topographies are highly sensitive both to the illumination mode and to the geometry of the object [15]. Second, Fig. 3 exhibits another interesting feature: As the observation distance is reduced, the corners and the metallic edges of the object appear to be enhanced compared to the central part of the metallic protrusion. This effect, specific to metallic objects, is consistent with the physical content of Eq. (14). Indeed, in the distance range studied here, the first Born approximation is perfectly valid. Under these conditions, it is easy to show that Γ is proportional to the imaginary part $\text{Im}[\mathbf{S}(\mathbf{r}_m, \mathbf{r}_m, \omega_0)]$ of the surrounding's propagator. For a metallic object, $\text{Im}[\mathbf{S}(\mathbf{r}_m, \mathbf{r}_m, \omega_0)]$ increases drastically at the immediate proximity of sharp edges and consequently reinforces the imaging contrast near localized regions that display the smallest curvature radius. Above the central part of the metallic island we have observed that the variation of the lifetime width remains significantly high, since η varies between 1.26 and 1.56 as the approach distance varies between 80 and 50 nm.

Finally, the numerical scheme described in this Letter could also be applied to other domains of electrodynamics, where the electromagnetic propagator of geometrically complex systems is required.

[1] K. H. Drexhage, H. Kuhn, and F. P. Schäfer, Ber. Bunsen-Ges. Phys. Chem. **72**, 329 (1968).
[2] M. R. Philpott, Chem. Phys. Lett. **19**, 435 (1973).
[3] H. Kuhn, J. Chem. Phys. **53**, 101 (1970).
[4] R. R. Chance, A. Prock, and R. Silbey, J. Chem. Phys. **60**, 2744 (1974).
[5] A. Harootunian, E. Betzig, M. Isaacson, and A. Lewis, Appl. Phys. Lett. **49**, 674 (1986).
[6] E. Betzig and J. K. Trautman, Science **257**, 189 (1992).
[7] E. Betzig and R. J. Chichester, Science **262**, 1422 (1994).
[8] X. S. Xie and R. C. Dunn, Science **265**, 361 (1994).
[9] W. P. Ambrose, P. M. Goodwin, J. C. Martin, and R. A. Keller, Science **265**, 364 (1994).
[10] W. E. Moerner, T. Plakhotnik, T. Irngartinger, D. W. Pohl, and B. Hecht, Phys. Rev. Lett. **73**, 2764 (1994).
[11] D. Barchiesi, T. Pagnot, Ch. Pieralli, and D. Van Labeke, Proc. SPIE Int. Soc. Opt. Eng. **2384**, 90 (1995).
[12] Ch. Girard, A. Dereux, and O. J. F. Martin, Surf. Sci. **295**, 445 (1993).
[13] An excellent and comprehensive overview about the "surface enhanced spectroscopy phenomena" can be found in H. Metiu, Prog. Surf. Sci. **17**, 153–320 (1982).
[14] Ch. Girard, A. Dereux, and O. J. F. Martin, Phys. Rev. B **49**, 13 872 (1994).
[15] D. Courjon, K. Sarayeddine, and M. Spajer, Opt. Commun. **71**, 23 (1989).
[16] O. J. F. Martin, Ch. Girard, and A. Dereux, Phys. Rev. Lett. **74**, 526 (1995).
[17] A. D. Maclachlan, R. D. Gregory, and M. A. Ball, Mol. Phys. **7**, 119 (1963).
[18] G. S. Agarwal, Phys. Rev. A **11**, 230 (1975).